Structure and properties of Mn₃O₄ thin films grown on single crystal substrates by chemical vapor deposition

Lorenzo Bigiani [a], Chiara Maccato [a,*], Alberto Gasparotto [a], Cinzia Sada [b], Davide Barreca [c]

[a] *Department of Chemical Sciences, Padova University and INSTM, 35131 Padova, Italy*

[b] *Department of Physics and Astronomy, Padova University and INSTM, 35131 Padova, Italy*

[c] *CNR-ICMATE and INSTM, Department of Chemical Sciences, Padova University, 35131 Padova, Italy*

* Corresponding author. Tel: +39-049-8275234, *E-mail address*: chiara.maccato@unipd.it (C. Maccato).

Abstract

Mn_3O_4 thin films were fabricated on $SrTiO_3(111)$ and $Y_3Al_5O_{12}(100)$ substrates by chemical vapor deposition (CVD) under O_2 atmospheres, starting from a fluorinated Mn(II) diketonate-diamine adduct. The obtained systems were investigated by a multi-technique characterization in order to elucidate the interplay between preparation conditions and their chemico-physical properties. The results highlighted the formation of phase-pure and homogeneous α-Mn_3O_4 (*haussmannite*) films, characterized by a smooth morphology, an appreciable Vis light absorption and structural features directly dependent on the used substrate. The target systems were uniformly doped with fluorine, due to the used Mn compound acting as a single-source precursor for both Mn and F. In addition, magnetic force microscopy measurements revealed the formation of spin domains and long-range magnetic order in the target materials, paving the way to their future implementation as magnetic media toward device integration for data storage.

1. Introduction

Mn_3O_4, one of the most stable manganese oxides, has a normal spinel structure characterized by the co-presence of Mn(II) (d^5) and Mn(III) (d^4) ions in the tetrahedral and octahedral crystal sites, respectively [1-2]. The presence of Mn(III) centers is responsible for a tetragonal distortion due to the Jahn-Teller effect [3-4]. Thanks to the interplay between spin, orbital, and lattice degrees of freedom [5], as well as to their high abundance and environmentally friendly nature, Mn_3O_4-based materials have attracted a great deal of attention for a variety of applications, including electrochemical capacitors, heterogeneous catalysts, sensors and magnetic storage devices [5-10].

To date, most studies have been performed on bulk and powdered Mn_3O_4 systems [11-18], rather than on the homologous thin films and supported nanomaterials, despite their great relevance for the fabrication of a multitude of devices/integrated systems [7,19]. In this context, a proper choice of the substrates plays a strategic role since their nature strongly affects the nucleation and growth processes of the forming system and its chemico-physical properties, leading, in turn, to diversified material performances as a function of specific target applications [20].

Up to date, the growth of Mn_3O_4 films by different fabrication methods has often been performed on polycrystalline substrates. In a different way, reports devoted to the growth of Mn_3O_4 thin films supported on single crystal substrates are so far limited [1,4-5,10], despite the structural, electronic and magnetic properties of the resulting oriented/epitaxial films are often superior than those of polycrystalline ones. In general, the use of single crystal substrates can not only stabilize specific polymorphs, but also impact on interface quality and surface faceting of the fabricated deposits [20], whose properties may be essentially different from their bulk counterparts and influence, in turn, the resulting functional behavior. On this basis, the development of synthetic strategies to control Mn_3O_4 deposition and the thorough

understanding of its growth on single crystals are of great importance from both a fundamental and an applied point of view.

In the present work, we report on the CVD of Mn_3O_4 thin films on $SrTiO_3(111)$ (STO) and $Y_3Al_5O_{12}$ (100) (YAO) substrates, used as examples to understand substrate influence on the deposited material chemico-physical properties. As a matter of fact, STO-based substrates have already been utilized for the growth of Mn_3O_4 films/nanosystems [1,4-5,7,19], whereas YAO-based ones have never been employed in this context. To the best of our knowledge, no studies regarding the CVD of Mn_3O_4 thin films on the target substrates are available in the literature so far. The use of the CVD technique stands as an amenable choice to control film properties under relatively mild conditions, without the need of exceedingly high temperatures and/or harsh conditions in terms of energy supply, ultra-high vacuum or complicated equipments. In this study, particular attention is devoted to the analysis of the system structure, chemical composition and optical properties as a function of the adopted substrate, as well as on the investigation of surface morphology and magnetic characteristics by the combined use of atomic force microscopy (AFM) and magnetic force microscopy (MFM). The results suggest the possibility of tuning film properties as a function of the adopted substrate and highlight the potential of the developed systems for eventual photocatalytic and magnetic applications.

2. Experimental

2.1 Synthesis

Manganese oxide thin films were fabricated *via* CVD by means of a custom-built cold-wall reactor [21], equipped with a quartz chamber and a resistively heated susceptor. $Mn(tfa)_2 \bullet TMEDA$ (Htfa = 1,1,1-trifluoro-2,4-pentanedione; TMEDA = *N,N,N',N'*-tetramethylethylenediamine), synthesized according to the literature [22], was used as molecular source. In each experiment, the precursor powders were vaporized at 65°C in an

external glass vessel heated by an oil bath and transported into the reactor by an electronic grade O_2 flow (rate = 100 standard cubic centimeters per minute (sccm)). The gas lines connecting the precursor reservoir and the reaction chamber were maintained at 105°C throughout each growth process by means of external heating tapes, in order to avoid undesired condensation phenomena and detrimental mass losses during precursor delivery. An additional O_2 flow (rate = 100 sccm) was separately introduced into the reaction chamber through an auxiliary inlet. Depositions were performed at a total pressure of 10.0 mbar for 1 h on as-received $SrTiO_3(111)$ and $Y_3Al_5O_{12}(100)$ substrates (CRYSTAL GmbH®, Berlin). Basing on previous experiments [23-24], the growth temperature was fixed at 400°C. At the end of each deposition process, the specimens were cooled down at room temperature under flowing O_2 before subsequent analyses.

2.2 Characterization

X-ray diffraction (XRD) patterns were collected on a Bruker D8 Advance diffractometer equipped with a Göbel mirror, using a CuKα source powered at 40 kV and 40 mA. Texture coefficients (TC), average crystallite dimensions (D), dislocation density (δ) and microstrain (ε) values were calculated following previous works [24-26]. Lattice parameters were obtained from (220) and (211) reflections [27].

Field emission-scanning electron microscopy (FE-SEM) images were taken on a Zeiss SUPRA 40VP instrument, using a primary beam acceleration voltage of 5.0 kV. The ImageJ® (http://imagej.nih.gov/ij/, accessed September 2017) software was used to estimate the average grain/domain size and deposit thickness.

Secondary ion mass spectrometry (SIMS) depth profiles were recorded by a Cameca IMS 4f instrument, using a Cs^+ beam (14.5 keV, 25 nA, stability: 0.3%) and negative ion detection. Measurements were performed in High Mass Resolution configuration, using an electron gun

for charge compensation. Signals were collected rastering over a 150×150 μm^2 area and detecting secondary ions from a sub-region close to 8×8 μm^2 to avoid crater effects. The signals were detected in beam blanking mode (*i.e.* interrupting the sputtering process during magnet stabilization periods) in order to improve the in-depth resolution. The sputtering time was converted into depth values using the film thickness data measured by cross-sectional field FE-SEM micrographs.

Optical absorption spectra were recorded in transmittance mode at normal incidence on a Cary 50 spectrophotometer, subtracting the substrate contribution in each case. Estimation of band gap values was performed by means of the Tauc procedure [20,28-29], assuming the occurrence of direct and allowed electronic transitions in Mn_3O_4 [22]. Although Tauc analysis was originally proposed for amorphous thin film materials, the method is robustly accurate and broadly applied even in the case of a variety of crystalline thin films grown on different substrates [20-22,25,28-30].

Surface morphology and magnetic properties were investigated by AFM and MFM, operating in contact and tapping mode respectively, using a NT–MDT SPM Solver P47H–PRO apparatus. Root Mean Square (RMS) roughness values were calculated from AFM images by the NT-MDT software, after background subtraction. Cantilever tips (average height = 15 µm) coated with a CoCr magnetic layer, pre-magnetized with an external field, were used for MFM analyses. The magnetic force was measured by monitoring phase shifts in cantilever oscillations, due to tip-sample magnetic interactions. Possible influence of electrostatic interactions was effectively reduced by sample discharging prior to each measurement.

3. Results and discussion

The system microstructural features were investigated by means of XRD analyses (Fig. 1a). The patterns of the target specimens, at variance with previous studies [6,19], indicated the

formation of phase-pure tetragonal *haussmannite* (α; space group: $I4_1/amd$, Fig. 1b), the most stable Mn_3O_4 polymorph [2,31]. The corresponding lattice parameters, calculated from (220) and (211) reflections [27] (a = 5.789 and 5.778 Å for Mn_3O_4/STO and Mn_3O_4/YAO, respectively; c = 9.236 and 9.210 Å for Mn_3O_4/STO and Mn_3O_4/YAO, respectively) were slightly higher (STO) and lower (YAO), respectively, than those of single crystal Mn_3O_4 (a = 5.762 Å and c = 9.470 Å [6,31]). These data indicated the occurrence of *x-y* in-plane elongation, along with *z* axis compression. Indeed, the c/a values (1.597 for Mn_3O_4/STO and 1.594 for Mn_3O_4/YAO) were smaller than the one of single crystal Mn_3O_4 (1.643), suggesting the occurrence of defects, like cation vacancies in octahedral sites. The latter, in turn, are responsible for a reduced *z*-axis Jahn-Teller distortion [3,5-6]. This compression was higher for Mn_3O_4/YAO, likely due to the different lattice mismatch between Mn_3O_4 and STO/YAO substrates [5], highlighting the substrate influence on the film microstructural characteristics. Additional information was obtained by the evaluation of texture coefficients (TC) [24,29] for (211) and (220) reflections. For both samples, the values of TC_{220} = 1.3 and TC_{211} = 0.7 highlighted a preferential (220) orientation, at variance with Si-supported samples [24], suggesting a direct substrate influence on material microstructure and growth mechanism. More specifically, crystallite dimensions (D), dislocation density (δ) and microstrain (ε) values [24] yielded D = 22 (26) nm, δ = 1.5×10^{15} (1.0×10^{15}) lines/m^2 and ε = 4.9×10^{-3} (4.0×10^{-3}) for Mn_3O_4/STO (Mn_3O_4/YAO). As can be observed, both the dislocation density and microstrain values decreased with an increase in the corresponding average crystallite dimensions (and also aggregate sizes estimated by FE-SEM analyses; see below), *i.e.* upon going from STO- to YAO-supported materials. This result, perfectly in line with previous works on thin films and nanosystems [24-26], suggested a lower defect content for materials grown on YAO, as indeed reflected by X-ray photoelectron spectroscopy (XPS) data (Supporting Information).

Subsequently, attention was devoted to analysing the system nano-organization by means of

FE-SEM. The obtained results revealed the formation of highly uniform thin films well adherent to the substrates (Figs. 1c-f), characterized by the presence of interconnected low-sized nanoaggregates endowed with a pseudo-spherical shape and mean dimensions directly dependent on the adopted growth substrate [(20 ± 5) and (25 ± 5) nm for Mn_3O_4/STO and Mn_3O_4/YAO, respectively, yielding thickness values of (150 ± 8) and (190 ± 10) nm in the two cases]. A comparison of the average aggregate sizes with the corresponding crystallite dimensions calculated from XRD patterns suggested that each particle was a single crystallite. The analysis of element chemical states by surface XPS investigation (Supporting Information) evidenced the obtainment of pure Mn_3O_4 deposits, free from the presence of other manganese oxides in appreciable amounts. An additional insight into the system composition was gained by SIMS in-depth profiles (Figs. 2a-b). After the initial F yield decrease due to the removal of CF_x precursor residuals (see the Supporting Information), a homogeneous fluorine dispersion throughout the investigated thickness was observed, irrespective of the used substrate. The parallel trends of Mn and F ionic yields highlighted that F introduction resulted from the used Mn complex, acting as a single-source precursor for both manganese and fluorine. This result could be of potential importance to modulate the system properties in various eventual applications [24]. In fact, fluorine doping enables to passivate surface defect states, enhancing the system surface reactivity and tailor its electrical properties, paving the way to various applications, from gas sensors to photocatalysts and magnetic devices [20,29].

Optical absorption spectra (Figs. 2c-d), in good agreement with previous works on Mn_3O_4 systems [3,6], exhibited a prominent absorption in the Vis region below 600 nm due to direct, allowed interband electronic transitions. The observed Vis light harvesting is of practical interest for light-triggered applications, such as sunlight-assisted water purification and photocatalytic H_2 generation [23]. The higher Mn_3O_4/YAO absorbance could be ascribed to its higher thickness (see above). The extrapolated optical band gaps [28] ($E_G = 2.35$ and 2.45 eV)

agreed to a good extent with previous literature data [22], confirming the formation of phase-pure Mn_3O_4.

Finally, the system surface morphology and magnetic properties were characterized using AFM and MFM, respectively, at room temperature and under ambient conditions (Fig. 3). Regardless of the substrate, AFM images confirmed the occurrence of a granular-like surface topography, with average particle sizes in line with FE-SEM results (see above) and RMS roughness values of 3.0 nm. A detailed inspection of FE-SEM images (Fig. 1) and AFM micrographs (Fig. 3) for the target systems suggested the possible occurrence of an island-type (Volmer–Weber) three-dimensional growth mode, yielding crystalline films comprising pseudo-spherical particles, endowed with a preferential (220) orientation (see above).

Furthermore, important information was gained by MFM measurements regarding the possible use of the developed materials at room temperature as magnetic media toward device integration for data storage. In this regard, an important applicative criterion to be satisfied is related to the magnetization stability down to the nanoscale, whose investigation requires to analyze the constitution and distribution of magnetic domains in the prepared nanosystems [32]. To this regard, MFM is a valuable and highly reliable technique. In the present case, the analyses evidenced an in-plane homogeneous distribution of magnetic domains. The reversing of MFM contrast from bright to dark regions corresponds to tip-surface interaction changing from repulsion to attraction, *i.e.* magnetic moments directed up and down, respectively [33]. These evidences suggested the occurrence of a long-range magnetic ordering [32]. The average diameters of magnetic domains were estimated to be 30 and 35 nm for Mn_3O_4/STO and Mn_3O_4/YAO specimens, respectively, indicating that they were formed by the aggregation of adjacent grains. The absence of large areas characterized by a single color enable to exclude the occurrence of magnetic impurities in appreciable amounts, further highlighting the effectiveness of the proposed fabrication route in the obtainment of pure Mn_3O_4 films with

controlled properties.

4. Conclusions

In this work, Mn_3O_4 thin films were grown by CVD on single-crystal $SrTiO_3(111)$ and $Y_3Al_5O_{12}(100)$ substrates. A multi-technique characterization evidenced the obtainment of single-phase *haussmannite* Mn_3O_4 deposits, with tailored morphology and nanoscale organization. In particular,the obtained results revealed the occurrence of a three-dimensional growth mode, yielding (220)-oriented crystalline films with pseudo-spherical particles and structural features directly affected by the adopted deposition substrate. The use of a fluorinated Mn(II) molecular source enabled to successfully achieve fluorine doping, with a uniform F content throughout film thickness. In addition, MFM analysis indicated the formation of spin domains with a long-range magnetic order. These findings, along with the prominent Vis light harvesting, are useful to synthesize Mn_3O_4 materials endowed with controlled properties. In particular, the used CVD route is flexible, solvent-free and amenable to scale-up, disclosing attractive perspectives for various applications, such as sunlight-driven photocatalysts for water and air purification and advanced magnetic devices. In this latter context, attractive perspectives for future research developments will concern a detailed investigation of Mn_3O_4 film magnetic properties and of their interplay with the adopted processing conditions. These issues will be the subject of our future attention.

technical support.

Appendix A. Supporting information

Supplementary data associated with this article (XPS analyses) can be found in the online version at http://dx.doi.org/10.1016/j.matlet.2016.XXX.

References

[1] S. Huang, Y. Wang, Z. Wang, K. Zhao, X. Shi, X. Lai, L. Zhang, Structural, magnetic and magnetodielectric properties of the Mn_3O_4 thin films epitaxially grown on $SrTiO_3$ (001) substrates, Solid State Commun. 212 (2015) 25-29.

[2] J. Zhang, J. Du, H. Wang, J. Wang, Z. Qu, L. Jia, A novel mild route to hausmannite Mn_3O_4 nanocubes at room temperature and its catalytic performance, Mater. Lett. 65 (2011) 2565-2567.

[3] V.C. Bose, V. Biju, Optical, electrical and magnetic properties of nanostructured Mn_3O_4 synthesized through a facile chemical route, Physica E 66 (2015) 24-32.

[4] O.Y. Gorbenko, I.E. Graboy, V.A. Amelichev, A.A. Bosak, A.R. Kaul, B. Guttler, V.L. Svetchnikov, H.W. Zandbergen, The structure and properties of Mn_3O_4 thin films grown by MOCVD, Solid State Commun. 124 (2002) 15-20.

[5] G. Wang, S. Wu, W. Zhou, Y. Wang, S. Li, Novel magnetic properties of single-crystalline Mn_3O_4 (004) film grown on $SrTiO_3$ (001) substrate by molecular beam epitaxy, Mater. Lett. 195 (2017) 86-88.

[6] V.C. Bose, V. Biju, Defect dependent optical, electrical and magnetic properties of nanostructured Mn_3O_4, Superlattices Microstruct. 88 (2015) 287-298.

[7] J. Liu, Y.H. Ng, M.B. Okatan, R. Amal, K.A. Bogle, V. Nagarajan, Interface-dependent electrochemical behavior of nanostructured manganese (IV) oxide (Mn_3O_4), Electrochim. Acta 130 (2014) 810-817.

[8] Y. Luo, T. Yang, Z. Li, B. Xiao, M. Zhang, High performance of Mn_3O_4 cubes for supercapacitor applications, Mater. Lett. 178 (2016) 171-174.

[9] M. Zhen, Z. Zhang, Q. Ren, L. Liu, Room-temperature synthesis of ultrathin Mn_3O_4 nanosheets as anode materials for lithium-ion batteries, Mater. Lett. 177 (2016) 21-24.

[10] J.Y. Liu, X. Cheng, V. Nagarajan, H.L. Xin, Understanding growth mechanisms of epitaxial manganese oxide (Mn_3O_4) nanostructures on strontium titanate (STO) oxide substrates, MRS Commun. 5 (2015) 277-284.

[11] C.-Y. Chen, Y.-R. Lyu, C.-Y. Su, H.-M. Lin, C.-K. Lin, Characterization of spray pyrolyzed manganese oxide powders deposited by electrophoretic deposition technique, Surf. Coat. Technol. 202 (2007) 1277-1281.

[12] N. Li, Y. Tian, J. Zhao, J. Zhang, J. Zhang, W. Zuo, Y. Ding, Efficient removal of chromium from water by Mn_3O_4@ZnO/Mn_3O_4 composite under simulated sunlight irradiation: synergy of photocatalytic reduction and adsorption, Appl. Catal., B 214 (2017) 126-136.

[13] H. Dong, E.K. Koh, S.-Y. Lee, Synthesis of Ag-Mn_3O_4 core-shell nanorods and Mn_3O_4 nanotubes from sacrificial Ag nanorod templates, J. Nanosci. Nanotechnol. 9 (2009) 6511-6517.

[14] N.N. Wang, J. Yue, L. Chen, Y.T. Qian, J. Yang, Hydrogenated TiO_2 branches coated Mn_3O_4 nanorods as an advanced anode material for lithium ion batteries, ACS Appl. Mater. Interfaces 7 (2015) 10348-10355.

[15] C. Chen, G.J. Ding, D. Zhang, Z. Jiao, M.H. Wu, C.H. Shek, C.M.L. Wu, J.K.L. Lai, Z.W. Chen, Microstructure evolution and advanced performance of Mn_3O_4 nanomorphologies, Nanoscale 4 (2012) 2590-2596.

[16] J.K. Sharma, P. Srivastava, S. Ameen, M.S. Akhtar, G. Singh, S. Yadava, *Azadirachta Indica* plant-assisted green synthesis of Mn_3O_4 nanoparticles: excellent thermal catalytic performance and chemical sensing behavior, J. Colloid Interface Sci. 472 (2016) 220-228.

[17] H. Rahaman, S. Kundu, S.K. Ghosh, Size-selective silver-Induced evolution of Mn_3O_4-Ag nanocomposites for effective ethanol sensing, ChemistrySelect 2 (2017) 6991-6999.

[18] J. Darul, C. Lathe, P. Piszora, Mn_3O_4 under high pressure and temperature: thermal stability, polymorphism, and elastic properties, J. Phys. Chem. C 117 (2013) 23487-23494.

[19] L. Ren, S. Wu, W. Zhou, S. Li, Epitaxial growth of manganese oxide films on $MgAl_2O_4$ (001) substrates and the possible mechanism, J. Cryst. Growth 389 (2014) 55-59.

[20] G. Carraro, A. Gasparotto, C. Maccato, E. Bontempi, O.I. Lebedev, C. Sada, S. Turner, G. Van Tendeloo, D. Barreca, Rational synthesis of F-doped iron oxides on Al_2O_3(0001) single crystals, RSC Adv. 4 (2014) 52140-52146.

[21] D. Barreca, A. Gasparotto, C. Maragno, E. Tondello, C. Sada, CVD of nanophasic (Zn,Cd)S thin films: from multi-layers to solid solutions, Chem. Vap. Deposition 10 (2004) 229-236.

[22] C. Maccato, L. Bigiani, G. Carraro, A. Gasparotto, R. Seraglia, J. Kim, A. Devi, G. Tabacchi, E. Fois, G. Pace, V. Di Noto, D. Barreca, Molecular engineering of Mn^{II} diamine diketonate precursors for the vapor deposition of manganese oxide nanostructures, Chem. Eur. J. 23 (2017) 17954-17963.

[23] D. Barreca, L. Bigiani, M. Monai, G. Carraro, A. Gasparotto, C. Sada, S. Martí-Sanchez, A. Grau-Carbonell, J. Arbiol, C. Maccato, P. Fornasiero, Supported Mn_3O_4 nanosystems for hydrogen production through ethanol photoreforming, Langmuir 34 (2018) 4568-4574.

[24] L. Bigiani, D. Barreca, A. Gasparotto, C. Sada, S. Marti-Sanchez, J. Arbiol, C. Maccato, Controllable vapor phase fabrication of $F:Mn_3O_4$ thin films functionalized with Ag and TiO_2, CrystEngComm 20 (2018) 3016-3024.

[25] A. Hakimyfard, S. Khademinia, M. Rahimkhani, Solid state synthesis, crystal structure, evaluation of direct and indirect band gap energies and optimization of reaction parameters for $As_2Ni_3O_8$ nanomaterials, J. Nanoanalysis 5 (2018) 91-98.

[26] P.V. Bhuvaneswari, K. Ramamurthi, R.R. Babu, Effect of substrate temperature on the structural, morphological and optical properties of copper bismuth sulfide thin films deposited by electron beam evaporation method, J. Mater. Sci.: Mater. Electron. 29 (2018) 17201-17208.

[27] J.P. Eberhart, Structural and Chemical Analysis of Materials, J. Wiley & Sons, New York, USA, 1995.

[28] G. Carraro, D. Peeters, A. Gasparotto, C. Maccato, E. Bontempi, D. Barreca, Fe_2O_3 nanostructures on $SrTiO_3$(111) by chemical vapor deposition: Growth and characterization, Mater. Lett. 136 (2014) 141-145.

[29] F. Yakuphanoglu, Y. Caglar, S. Ilican, M. Caglar, The effects of fluorine on the structural, surface morphology and optical properties of ZnO thin films, Physica B 394 (2007) 86-92.

[30] B.D. Viezbicke, S. Patel, B.E. Davis, D.P. Birnie, Evaluation of the Tauc method for optical absorption edge determination: ZnO thin films as a model system, Phys. Status Solidi B 252 (2015) 1700-1710.

[31] Pattern N° 024-0734, JCPDS (2000).

[32] S. Chandra, R. Das, V. Kalappattil, T. Eggers, C. Harnagea, R. Nechache, M.-H. Phan, F. Rosei, H. Srikanth, Epitaxial magnetite nanorods with enhanced room temperature magnetic anisotropy, Nanoscale 9 (2017) 7858-7867.

[33] V. Strelchuk, O. Kolomys, S. Rarata, P. Lytvyn, O. Khyzhun, C.O. Chey, O. Nur, M. Willander, Raman submicron spatial mapping of individual Mn-doped ZnO nanorods, Nanoscale Res. Lett. 12 (2017) 351.

Captions for Figures

Figure 1   (a) XRD patterns of manganese oxide thin films deposited on STO and YAO substrates. (b) Representation of the α-Mn_3O_4 (*haussmannite*) structure [31]. Plane-view and cross-sectional FE-SEM images of Mn_3O_4 films supported on STO (c,e) and YAO (d,f).

Figure 2   SIMS depth profiles for Mn_3O_4 films deposited on STO (a) and YAO (b). Optical absorption spectra (c) and Tauc plots (d) obtained with $n = 2$ (direct and allowed transitions) [22,28].

Figure 3   AFM/MFM micrographs and corresponding line scans along the marked lines for Mn_3O_4 specimens deposited on STO (a) and YAO (b).
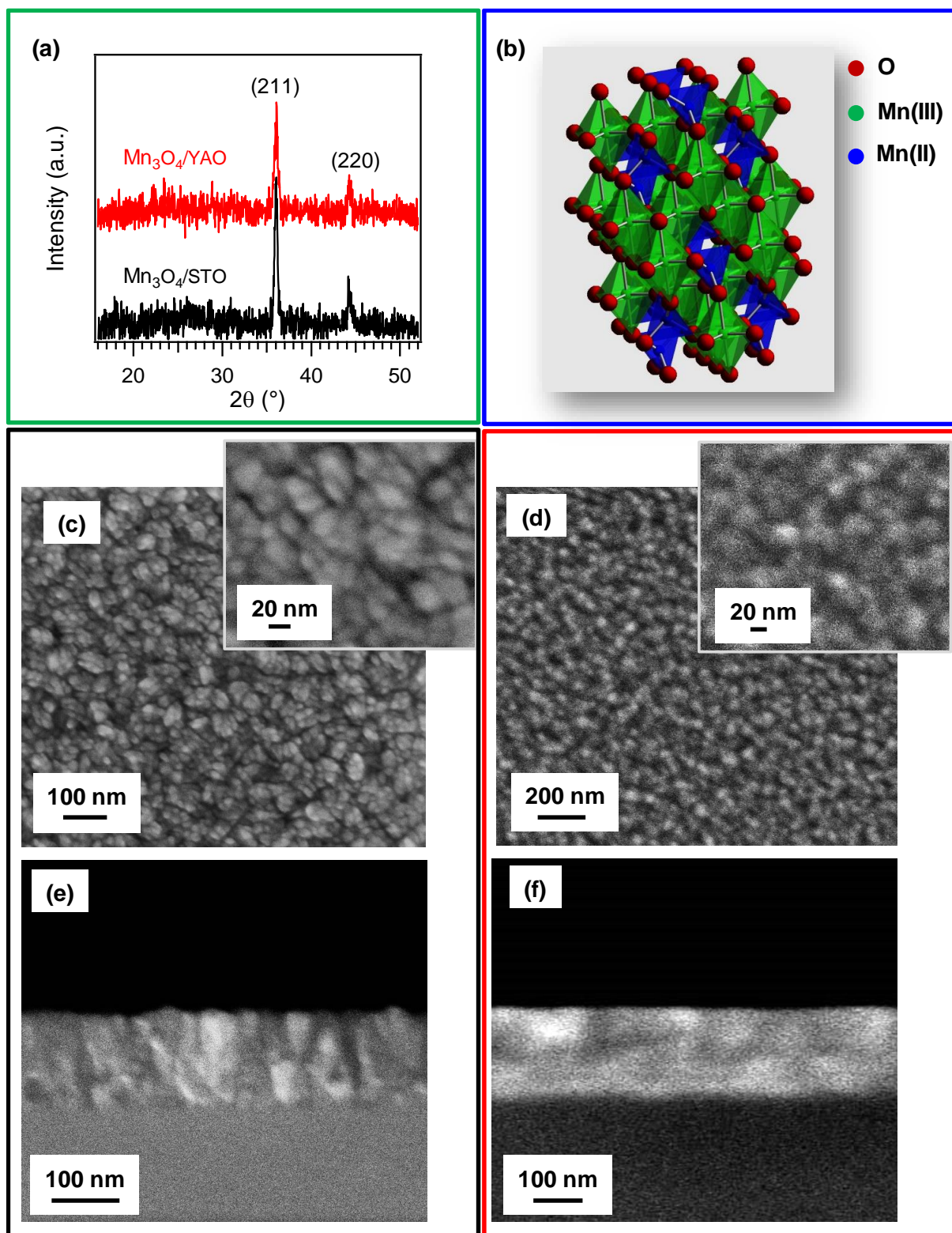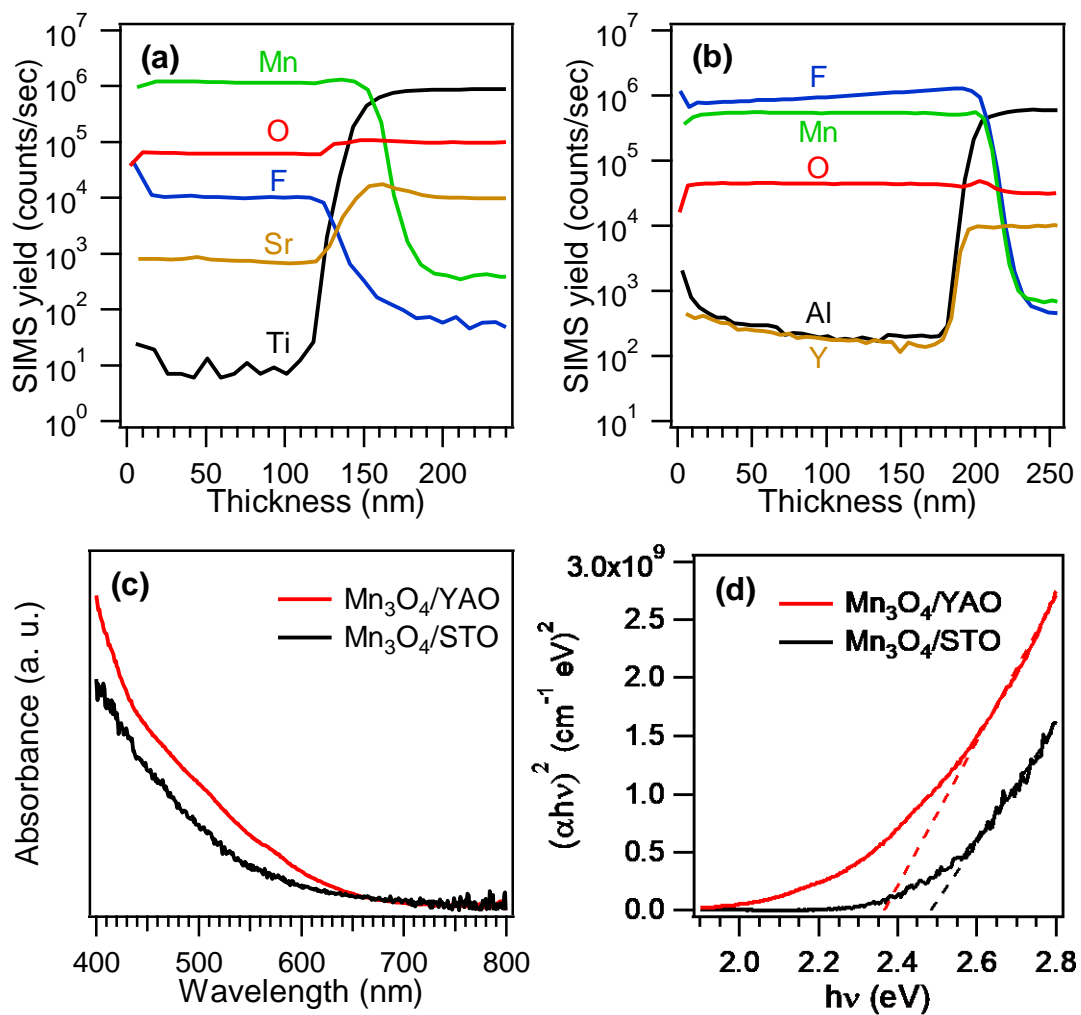
Figure 1

by L. Bigiani *et al.*

Figure 2

by L. Bigiani *et al.*

Figure 3

by L. Bigiani *et al.*